Asymptotic normalization coefficients for ^{7}Be + $p \rightarrow {}^8$B from the peripheral ^{7}Be(d,n)^{8}B reaction and their astrophysical application

O. R. Tojiboev,[1] R. Yarmukhamedov,[1,*] S. V. Artemov,[1] and S. B. Sakuta[2]
[1]*Institute of Nuclear Physics, Academy of Sciences of the Republic of Uzbekistan, Tashkent 100214, Uzbekistan*
[2]*National Research Center "Kurchatov Institute," Moscow 123182, Russia*
(Received 16 February 2016; revised manuscript received 10 August 2016; published 17 November 2016)

The proton transfer ^{7}Be(d,n)^{8}B reaction at the energy of 4.5 MeV (center of mass) has been analyzed within the modified distorted-wave Born approximation. New estimates and their uncertainties are obtained for values of the asymptotic normalization coefficients for $p + {}^7\text{Be} \rightarrow {}^8$B, the astrophysical $S_{17}(0)$ factor, and the s-wave $p + {}^7$Be scattering lengths.

DOI: 10.1103/PhysRevC.94.054616

I. INTRODUCTION

The radiative capture ^{7}Be(p,γ)^{8}B reaction rate given in terms of the extremely low energy astrophysical S factor is one of the main input data for calculations of the solar-neutrino flux [1–6]. At the stellar temperature $T_6 \sim 15$ K, this rate determines how much the ^{7}Be and ^{8}B branches of the pp chain contribute to the hydrogen burning. In the standard solar model, the predicted flux of neutrinos is determined by the relation [1]

$$\phi_\nu \sim \tilde{S}_{11}^{-2.5}\tilde{S}_{33}^{-0.3}\tilde{S}_{34}^{0.8}\left[1 + 3.47\tilde{S}_{17}\tilde{\tau}_{e7}^{-1}\right]. \quad (1)$$

Here $\tilde{S}_{ij} = S_{ij}(E)/S_{ij}(0)$ and $\tilde{\tau_{e7}} = \tau_{e7}(E)/\tau_{e7}(0)$, where $S_{ij}(E)$ is the extremely low energy astrophysical S factor for the reactions of the pp chain induced by collisions of the nuclei with mass numbers i and j, $\tau_{e7}(E)$ is the ^{7}Be lifetime with respect to the electron capture $^7\text{Be} + e^- \rightarrow {}^7\text{Li} + \nu_e$ reaction, and E is the relative kinetic energy of the colliding particles. It is seen that the flux of neutrinos depends noticeably on the β decay of ^{8}B determined in turn by the accuracy of the astrophysical S factors of the ^{7}Be(p,γ)^{8}B reaction at so-far experimentally inaccessible solar energies ($E \lesssim 25$ keV), including $E = 0$.

It is known that the uncertainty in extrapolation of the astrophysical S factors to the Gamow energy $E_G = 18$ keV obtained at the stellar temperature $T_6 = 15$ K (Sun) [7] affects significantly the predicted flux of solar ^{8}B neutrinos [6,8].

Despite the impressive improvements in our understanding the nuclear-astrophysical ^{7}Be(p, γ)^{8}B reaction made in a period of 10 consecutive years, some ambiguities connected with both the extrapolation of the astrophysical S factors to the solar energy region and the theoretical prediction for $S_{17}(E)$ still exist and can influence the prediction of the standard solar model [6]. For example, the analysis of the precisely measured astrophysical S factors for the ^{7}Be(p, γ)^{8}B reaction and their extrapolation performed by different authors from the observed energy regions to extremely low experimentally inaccessible energies gives values of $S_{17}(0)$ with a spread exceeding noticeably the experimental ones (see the recent reviews [8,9] and references therein as well as Ref. [10]). As regards the theoretical microscopic calculations of $S_{17}(0)$, they also show considerable spread connected with the method used (see, for example, Refs. [11–13] and the available references therein). It should be noted that a considerable sensitivity of the calculated value of $S_{17}(0)$ is observed in Refs. [11–13] to the used effective nucleon-nucleon (NN) potential. Moreover, as is evident from these works, a correlation has been revealed between the asymptotic normalization coefficients (ANC) calculated for $p + {}^7\text{Be} \rightarrow {}^8$B, which determine the amplitude of the tail of the radial ^{8}B nucleus bound wave function in the ($^7\text{Be} + p$) channel [14], and the calculated $S_{17}(0)$.

Taking into account this fact, in the past few years several works have been performed to determine the ANC for $p + {}^7\text{Be} \rightarrow {}^8$B and the $S_{17}(0)$ with an accuracy as high as possible. In Ref. [10], the "indirectly determined" value of ANCs for $^7\text{Be} + p \rightarrow {}^8$B were obtained by means of the analysis of the precisely measured experimental astrophysical S factors [$S_{17}^{\text{exp}}(E)$] performed within the modified two-body potential approach (MTBPA) [15], where $S_{17}(E)$ for the direct radiative capture ^{7}Be(p, γ)^{8}B reaction is expressed in terms of ANC for $p + {}^7\text{Be} \rightarrow {}^8$B. Then the derived ANC was used for extrapolation of the corresponding astrophysical S factors to solar energies. In Ref. [16] (see also Refs. [17,18]), the ANC values for $p + {}^7\text{Be} \rightarrow {}^8$B were obtained from analysis of the peripheral proton transfer ^{10}B(^{7}Be ,^{8}B)^{9}Be and ^{14}N(^{7}Be ,^{8}B)^{13}C reactions. The analysis was performed within the modified distorted-wave Born approximation (DWBA) restricting by the first order of the perturbation theory over the Coulomb polarization potential (ΔV_f^C) in the transition operator and assuming that its contribution to the total transition operator is small. But the ANC values proposed in Ref. [16] may not have sufficient accuracy because of the aforementioned assumption made for the transition operators [19,20]. Nevertheless, in Ref. [16] the obtained ANC values were then used for the estimation of $S_{17}(0)$, which also differs noticeably from that recommended in Refs. [8,10,21]. As noted in Refs. [10,20], one of the main reasons of the observed discrepancy is connected with underestimated values of the ANCs suggested in Ref. [16] as compared with that obtained in Refs. [10,20].

This disagreement initiated a number of the new measurements of other kinds of peripheral nuclear processes to obtain an additional information about the ANC values for $^7\text{Be} + p \rightarrow {}^8$B and their astrophysical application. Particularly, the analysis of the experimental differential cross sections for the peripheral proton transfer ^{7}Be(d,n)^{8}B reaction,

*Corresponding author: rakhim@inp.uz

measured in inverse kinematics at the energies 5.8 [22] and 4.5 MeV [23] in the center-of-mass system (denoted by E_i everywhere below), was performed in Refs. [22–24]. In Refs. [22–24], the analysis was carried out within the standard DWBA and the three-body approach with the effects of breakup of the deuteron in the field of the target treated by means of the continuum-discretized coupled-channel method (CDCCM). There the calculated cross sections are expressed in terms of the spectroscopic factors for the ^{8}B nucleus in the (^{7}Be + p) configuration. Besides, in Ref. [22], for the transferred proton only the $1p_{3/2}$ configuration was taken into account. However, in Refs. [22–24] the extracted spectroscopic factors, used for obtaining the ANC values, may not be accurate enough. This is connected with the fact that the calculated single-particle cross sections, as will be shown below, become very sensitive to the adopted values of the geometric parameters of the Woods-Saxon potential used for calculation of the bound- ^{8}B[= (^{7}Be + p)] state wave function [25]. The calculations of the ^{7}Be(d,n)^{8}B reaction [22,23] done in Ref. [26] within the strict Faddeev-type three-body (n, p, and ^{7}Be) equations should be noted. In Ref. [26], the realistic Bonn and several parametrization for the core-nucleon potentials were used as np and nucleon-core potentials, respectively. Nevertheless, the spectroscopic factors for single-component states of the nuclei were assumed to be unity. In this approximation, the ANC values for ^{7}Be + $p \to {}^8$B become model dependent on the geometric parameters of the used potential. One notes that the potential used in Ref. [26] for the bound (^{7}Be + p) state has the Woods-Saxon form with the central and spin-orbit parts for which the standard values for the geometric parameters ($r_o = 1.25$ fm and $a = 0.65$ fm) were taken.

The results of the analysis of the experimental differential cross sections [22] of the ^{7}Be(d,n)^{8}B reaction obtained in Ref. [27] within the modified DWBA [28–30], where the differential cross section is expressed in terms of the ANC but not in terms of the spectroscopic factors, should also be noted. In Ref. [27], the ANC values for ^{7}Be + $p \to {}^8$B were obtained by using the optical potentials recommended in Ref. [22] for the entrance and exit channels, but contribution of the compound nucleus evaluated in Ref. [22] and the coupled channels effects were not taken into account. So, it should be noted that, first, the experimental data of Ref. [22] in the main peak region of the angular distribution have fairly large errors not only in the absolute values of the differential cross sections but also in the angle resolution. Second, as is shown in Ref. [23], calculations with the optical parameters of Ref. [22] for the entrance channel, which are also used in Ref. [27], reproduce the corresponding experimental scattering data only in a narrow angular interval of the forward hemisphere. Therefore, the ANC values of Ref. [27] also may not have enough accuracy for the astrophysical application.

It is therefore of great interest to apply the modified DWBA for the analysis of the experimental data of the ^{7}Be(d,n)^{8}B reaction measured in Ref. [23] since they are more peripheral and more precise than the data of Ref. [22].

In the present work, the reanalysis of the ^{7}Be(d,n)^{8}B reaction at energy $E_i = 4.5$ MeV [23] is performed within the modified DWBA [28–30] to obtain the "indirectly determined" values of the ANC for ^{7}Be + $p \to {}^8$B, which were then used for estimation of the $S_{17}(0)$. Here, we quantitatively show that the ^{7}Be(d,n)^{8}B reaction measured in Ref. [23] is practically peripheral in the main peak region of the angular distribution. Therefore, the uncertainties, which are connected both with the ambiguities of choice of the geometric parameters (radius r_o and diffuseness a) of the Woods-Saxon potential used for calculating of the bound-state wave functions and with choice of the parameter set of optical potentials, are reduced to the physically acceptable limit, being within the errors of the analyzed experimental differential cross sections.

II. ANALYSIS OF THE ^{7}Be(d,n)^{8}B REACTION

A. The basic formulas of the modified DWBA

Here we present only the main idea and the essential formulas of the modified DWBA [29,30] specialized for the ^{7}Be(d,n)^{8}B reaction.

Let us write $l_B(j_B)$ for the orbital (total) angular momentum of the proton in the ^{8}B nucleus and $l_d(j_d)$ for the proton in the deuteron. For the ^{7}Be(d,n)^{8}B reaction, the value of l_B is taken to be equal to 1 and the values of j_B are taken to be equal to 1/2 and 3/2, while the values l_d and j_d are taken equal to 0 and 1/2 for s wave and to 2 and 3/2 for d wave, respectively.

In the strict three-body (^{7}Be , p, and n) approach, the transition operator for the amplitude of the ^{7}Be(d,n)^{8}B reaction, which is sandwiched between the products of the corresponding optical and bound-state wave functions in the initial and final states, has the form [31,32]

$$V^{\mathrm{TB}} = \Delta V_f^N + \Delta V_f^N G \Delta V_i. \tag{2}$$

Here G is the operator of the three-body (^{7}Be , p, and n) Green function, which takes into account all possible subsequent elastic rescatterings of the nucleus ^{7}Be, p, and n in the intermediate state, $\Delta V_f^N = V_{pn}^N + V_{n\mathrm{Be}}^N - V_f^N$, $\Delta V_i = V_{n\mathrm{Be}}^N + V_{p\mathrm{Be}} - V_i$, where $V_{ij} = V_{ij}^N + V_{ij}^C$, $V_{ij}^N(V_{ij}^C)$ is the nuclear (Coulomb) potential between the center of mass of particles i and j, which does not depend on the coordinates of the constituent nucleus, V_i and V_f^N are the optical Coulomb-nuclear and pure nuclear potentials in the initial and final states, respectively. The first (V_{pn}^N) and second ($V_{n\mathrm{Be}}^N$) terms entering the first term of the right-hand side of (2) correspond to the mechanisms described by the pole and triangle diagrams in Figs. 1(a) and 1(b), respectively, where in the latter diagram the core-core nuclear scattering is taken into account in the Born approximation for the amplitude of the four-ray vertex. The last term in the right-hand side of (2) corresponds to the more complex mechanisms than the pole and triangle ones.

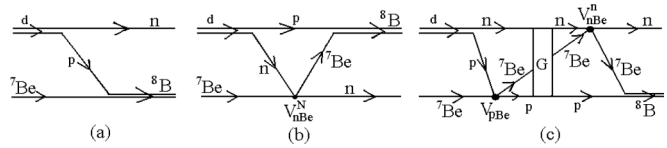

FIG. 1. Diagrams describing transfer of the proton p and taking into account possible subsequent Coulomb-nuclear rescattering of particles (^{7}Be, p, and n) in the intermediate state.

This term is described by a sum of nine diagrams obtained from the basic diagrams presented in Figs. 1(a) and 1(b) by means of all possible elastic rescatterings the nucleus ^{7}Be, p, and n from each other in the intermediate state. One of the nine diagrams corresponding to the term $V^N_{n\mathrm{Be}} G V_{p\mathrm{Be}}$ is plotted in Fig. 1(c). This term corresponds to the mechanism of subsequent rescattering of ^{7}Be on the proton and neutron virtually emitted by deuteron in the intermediate state.

Nevertheless, if the reaction under consideration is peripheral, then its dominating mechanism, at least in the main peak of the angular distribution, corresponds to the pole diagram Fig. 1(a) [33]. In this case, the contribution of the remnant $V^N_{n\mathrm{Be}} - V^N_f$ from the first term in the right-hand side of Eq. (2) is assumed fairly small and that of the second term $(\Delta V^N_f G \Delta V_i)$ in V^{TB} (2) can be ignored since its contribution is a higher order of smallness than the remnant $V^N_{n\mathrm{Be}} - V^N_f$ term. Then the single-particle DWBA cross section corresponding to the main mechanism can be calculated within the finite-range DWBA in the "post"-approximation with the DWUCK5 code. Besides, in this case, the influence of ambiguity of the optical model parameters on the calculated single-particle DWBA cross section should be small, at least not exceeding the experimental errors. In this case, the largest uncertainty in the single-particle DWBA cross section comes from its strong dependence on the geometric parameters (radius r_0 and diffuseness a) of the Woods-Saxon potential used for calculating the single-particle ^{8}B[$=(^7\mathrm{Be}+p)$] bound-state wave function. It is known that this dependence enters the single-particle DWBA cross section mainly through the corresponding single-particle ANC [25]. It will be demonstrated below that the reaction ^{7}Be$(d,n)^8$B at $E_i = 4.5$ MeV is peripheral, so the single-particle ANCs for the shell-model bound wave functions of the residual nucleus ^{8}B, entering the calculated single-particle DWBA cross section, are the free parameters.

Only the s wave is taken into account for the deuteron wave function in our calculations. This approximation is justified by the fact that the reaction under consideration has the peripheral character at least in the main peak region of the angular distribution. Therefore, in this angle region, the dominant contribution to the DWBA cross sections comes from the surface and outer regions of the colliding nuclei. In this interaction region, contribution of the d-wave component of the deuteron wave function to the calculated DWBA cross sections is strongly suppressed and can be ignored as compared to that for the s wave [14,34] since the amplitude of the "tail" determined by the corresponding ANC of the d wave is very small ($C_{d;3/2} = 2.29 \times 10^{-2}$ fm$^{-1/2}$ [14]). Besides, the additional suppression of this contribution occurs due to the kinematic factor of $(\kappa_d r_{np})^{-l_d}$ arising at $l_d = 2$ in the integrand for the matrix element since $\kappa_d r_{np} \gg 1$ for the peripheral reaction. Here κ_d is the wave number of deuteron and r_{np} is a relative distance between proton and neutron (see below).

Then, according to Refs. [28–30], within the modified DWBA, we can write the differential cross section in the form

$$\frac{d\sigma}{d\Omega} = C^2_{B;3/2} C^2_{d;1/2} [\mathcal{R}_{3/2\ 1/2}(E_i,\theta;\ b_{B;3/2},b_{d;1/2}) + \lambda \mathcal{R}_{1/2\ 1/2}(E_i,\theta;\ b_{B;1/2},b_{d;1/2})], \tag{3}$$

$$\mathcal{R}_{j_B j_d}(E_i,\theta;\ b_{B;\,j_B},b_{d;1/2}) = \frac{\sigma^{\mathrm{DW}}_{j_B j_d}(E_i,\theta;\ b_{B;\,j_B},b_{d;1/2})}{b^2_{d;1/2} b^2_{B;\,j_B}}, \tag{4}$$

where $C_{d;\,j_d}$ ($j_d = 1/2$) and $C_{B;\,j_B}$ ($j_B = 1/2$ and $3/2$) are the ANCs for $p + n \to d$ and $^7\mathrm{Be} + p \to {}^8$B, respectively, $\lambda = (C_{B;1/2}/C_{B:3/2})^2$, E_i is the relative kinetic energy of the colliding particles and θ is the scattering angle in center of mass. In Eqs. (3) and (4), $b_{B;\,j_B}$ is the single-particle ANCs for the shell-model wave function for the bound $(^7\mathrm{Be}+p)$ state, which determine the amplitude of its tail [14]; $b_{d;\,j_d}$ is the amplitude of the tail of the s-wave deuteron wave function of relative motion of the neutron and proton in the deuteron ($j_d = 1/2$); and $\sigma^{\mathrm{DW}}_{j_B j_d}(E_i,\theta;\ b_{B;\,j_B},b_{d;1/2})$ is the single-particle DWBA cross section. For independent testing, the single-particle DWBA cross section has been calculated also using the LOLA codes [35] restricted only by the first-order perturbation term over ΔV^C_f in the transition operator. Both calculations gave practically the same results since $\Delta V^C_f = 0$.

One notes that the spectroscopic factor ($Z^{1/2}_{B;\,j_B}$), which is a norm of the radial overlap function of the bound-state ^{8}B wave function in the $(^7\mathrm{Be}+p)$ channel, is related to the ANC $C_{B;\,j_B}$ by the equation [14]

$$C_{B;j_B} = Z^{1/2}_{B;\,j_B} b_{B;\,j_B}. \tag{5}$$

The same relation holds for the ANC $C_{d;j_d}$ and the spectroscopic factor $Z_{d;\,j_d}$. By inserting these relations into Eqs. (3) and (4), the differential cross section can be expressed in terms of the product of $Z_{B;\,j_B} Z_{d;\,j_d}$ used in the conventional DWBA (see, for example, Ref. [24]). Thus, the conventional DWBA and the modified DWBA differed from each other only by a choice of the form of parametrization for the differential cross section. However, for the reaction under consideration the modified DWBA should be used. Only in this case, the problem of the ambiguity, connected with the strong dependence of the calculated cross section on the geometric parameters of the adopted potentials, is removed by inclusion of the information about the ANCs for $^7\mathrm{Be} + p \to {}^8$B and $p + n \to d$. As it will be shown below, the latter reduces this ambiguity to minimum, at least, within the experimental errors for the cross-section data.

In (3), the ANC $C_{B;3/2}$, the single-particle ANCs $b_{B;\,j_B}$ ($j_B = 1/2$ and $3/2$) and the parameter $b_{d;1/2}$ are unknown, whereas the values of the ANC $C^2_{d;1/2}(= 0.774 \pm 0.018$ fm^{-1} [14,34]) for $p + n \to d$ and $\lambda(= 0.125$ [16,36]) $^7\mathrm{Be} + p \to {}^8$B are known. One notes that the "experimental" value of the ANC $C^2_{d;1/2}$ is in excellent agreement with that

calculated by different forms of the realistic NN potential where its value was found insensitive to the used form of the potential (see Ref. [14] for example). This circumstance makes it possible to calculate the deuteron wave function by using the Woods-Saxon potential.

To make the dependence of the $\mathcal{R}_{j_B\,1/2}(E_i,\theta;\, b_{B;\,j_B},b_{d;\,1/2})$ function on $b_{B;\,j_B}$ more transparent, we have restricted only by the main term (V^N_{np}) in the right-hand side of (2) and used the zero-range version of DWBA for the V^N_{np} potential with fixed optical model parameters in the initial and final states. Note that this consideration is also valid for the finite range of DWBA. In the radial integral for the matrix element [32] in the $\mathcal{R}_{j_B\,1/2}(E_i,\theta;\, b_{B;\,j_B},b_{d;\,1/2})$ function we split the space of interaction of the colliding particles into two parts separated by the channel radius $R_{\rm ch}$ [25]: the interior part ($0 \leqslant R \leqslant R_{\rm ch}$), where nuclear forces between the colliding nuclei are important, and the exterior part ($R_{\rm ch} \leqslant R < \infty$), where the interaction between the colliding nuclei is governed by Coulomb forces only. The exterior part of the radial integral for the matrix element in the $\mathcal{R}_{j_B\,1/2}(E_i,\theta;\, b_{B;\,j_B},b_{d;\,1/2})$ function does not contain explicitly the free parameter $b_{B;\,j_B}$, since for $R > R_{\rm ch}$ the bound- [(^{7}Be + p)] state wave function $\varphi_{B;\,j_B}(R)\,(=\varphi_{B;\,j_B}(R;b_{B;\,j_B})$ [25]) can be approximated by its asymptotic behavior [14]. Consequently, parametrization of the differential cross section in the form (3) allows us to fix the contribution from the exterior region in a model-independent way, if it is dominant for the peripheral reaction and if the ANCs $C_{B;\,j_B}$ ($j_B = 1/2$ and $3/2$) are known. In that case, the contribution from the interior part of the radial matrix element to the $\mathcal{R}_{j_B\,1/2}(E_i,\theta;\, b_{B;\,j_B},b_{d;\,1/2})$ function, which depends on $b_{B;\,j_B}$ through the fraction $\varphi_{B;\,j_B}(R;b_{B;\,j_B})/b_{B;\,j_B},b_{d;\,1/2}$ [25,32], exactly determines the dependence of the $\mathcal{R}_{j_B\,1/2}(E_i,\theta;\, b_{B;\,j_B},b_{d;\,1/2})$ function on $b_{B;\,j_B}$. It should be noted that this fraction is convolved with the radial optical wave functions in the initial and final states in the integrand of the radial integral for the interior part of the matrix element. The contribution from the interior part to the $d\sigma/d\Omega$ cross section is determined by the free parameters $b_{B;\,j_B}$ and the spectroscopic factors $Z_{B;\,j_B}$ through the product of $Z^{1/2}_{B;\,j_B}\varphi_{B;\,j_B}(R;b_{B;\,j_B})$, which is really model dependent due to the unknown free parameters $b_{B;\,j_B}$. As is seen from here and will be demonstrated below, at the fixed available "indirectly determined" values of the ANCs $C_{B;j_B}$ and $C_{d;j_d}$ (see Table IV), ambiguity of single-particle ANC values $b_{B;\,j_B}$ leads to the large uncertainty in the absolute values of the spectroscopic $Z_{B;\,j_B}$ factors. Besides, as a rule, this inaccuracy for $Z_{B;\,j_B}$ can also grow because of optical potentials ambiguities arising mainly in the interior part of the matrix element. Apparently, the analogous situation may occur for the other nucleon transfer reactions induced by a deuteron, including the reactions systematically studied in Ref. [37] taking into account the deuteron's breakup in the field of the target. It should be noted that for small relative distances between colliding light nuclei, which are responsible for the low partial-wave amplitudes corresponding to the processes proceeding inside nuclei, the optical model potentials cannot, generally speaking, reflect the true nature of many-particle nuclear interactions [30]. Therefore, the dependence on the single-particle ANCs and optical model potentials in the interior part of the matrix element can be one of the main reasons of the strong dependence of empirical ("experimental") values of the spectroscopic factors $Z_{B;\,j_B}$ extracted from different forms of the DWBA analysis (see Refs. [20,24]).

Nevertheless, if the ^{7}Be$(d,n)^8$B reaction is peripheral in the angular region near the main peak the contribution of the internal part into the $\mathcal{R}_{j_B\,1/2}(E_i,\theta;\, b_{B;\,j_B},b_{d;\,1/2})$ must be strongly suppressed. In this case, Eq. (3) can be used for determination of the square ANCs $C^2_{B;\,j_B}$, since, in the external part of the matrix element, the optical potential ambiguity and the dependence of the $\mathcal{R}_{j_B\,1/2}(E_i,\theta;\, b_{B;\,j_B},b_{d;\,1/2})$ function on $b_{B;\,j_B}$ can be reduced to minimum. To this end, according to Ref. [28], at the fixed values of $C^2_{d;\,1/2}$, λ and optical model parameters for the initial and final states, obviously the peripheral character for the ^{7}Be$(d,n)^8$B reaction is conditioned by

$$\mathcal{R}_{j_B\,1/2}(E_i,\theta;\, b_{B;\,j_B},b_{d;\,1/2}) = f(E_i,\theta), \tag{6}$$

where the left-hand side of Eq. (6) should not depend on $b_{B;\,j_B}$ and $b_{d;\,1/2}$ for each fixed energy E_i and scattering angle θ belonging to the main peak. Then, from (3) and (6), the following condition:

$$C^2_{B;3/2} = \frac{d\sigma/d\Omega}{C^2_{d;\,1/2}[\mathcal{R}_{3/2\;1/2}(E_i,\theta;\, b_{B;3/2},b_{d;\,1/2}) + \lambda\mathcal{R}_{1/2\;1/2}(E_i,\theta;\, b_{B;1/2},b_{d;\,1/2})]} = \text{const} \tag{7}$$

must be fulfilled for each fixed energy E_i, θ, and the function of $\mathcal{R}_{j_B}(E_i,\theta;\, b_{B;l_B j_B},b_{d;\,1/2})$ from (6).

Thus, introduction of the conditions (6) and (7) into the DWBA analysis guarantees the correct absolute normalization of the peripheral reaction cross section and supports the assumption about the dominance of the peripheral character of the proton transfer within (or near) the main peak of the angular distribution, which is mainly determined by the true peripheral partial-wave amplitudes at $l \gg 1$ [19]. Therefore, fulfillment (or weak violation within the errors of the experimental differential cross section $d\sigma^{\rm exp}/d\Omega$) of the conditions (6) and (7) makes it possible to obtain the experimental ("indirectly determined") value of squared ANC $(C^{\rm exp}_{B\,j_B})^2$ for ^{7}Be $+p \to {}^8$B using the $d\sigma^{\rm exp}/d\Omega$, measured in the main peak of the angular distribution, for $d\sigma/d\Omega$ and the value of $C^2_{d;\,1/2}$ [14,34].

B. Asymptotic normalization coefficients for ^{7}Be + $p \to {}^8$B

To determine the ANC values for ^{7}Be $+ p \to {}^8$B, the experimental differential cross sections measured in inverse kinematics for the ^{7}Be$(d,n)^8$B reaction at the energy of $E_i = 4.5$ MeV [23] were reanalyzed by the modified DWBA.

TABLE I. Parameters of the optical potentials corresponding to the entrance (a) and exit (b) channels for the ^{7}Be(d,n)^{8}B reaction at the energies $E_d = 5.79$ and 7.46 MeV in the laboratory system.

E_d, (MeV)	Set	Channel	V, (MeV)	r_V, (fm)	a_V, (fm)	$4W_D(W)$, (MeV)	$r_D(r_W)$, (fm)	$a_D(a_W)$, (fm)	V_{so}, (MeV)	r_{so}, (fm)	a_{so}, (fm)
5.79	1	a	72.0	1.05	0.95	(30.00)	(0.84)	(0.85)	12.8	1.05	0.94
		b	28.0	1.64	1.05	121.2	1.94	0.11	4.9	1.64	0.27
	2	a	67.0	1.35	0.93	18.00	2.48	0.30	16.0	0.86	0.25
		b	47.1	1.31	0.66	33.52	1.26	0.48			
	3	a	66.2	1.35	0.93	17.43	2.43	0.30	16.0	0.86	0.25
		b	35.8	1.51	0.43	25.98	1.84	0.51	5.8	1.18	0.51
	4	a	64.0	1.35	0.90	18.68	2.37	0.30	12.0	0.86	0.25
		b	35.8	1.51	0.43	25.98	1.84	0.51	5.8	1.18	0.51
7.46	1a	a	65.0	1.35	0.89	19.16	2.34	0.30	12.0	0.86	0.25
		b	48.19	1.20	0.72	30.32	1.43	0.66	5.2	1.13	0.77
	2a	a	64.0	1.35	0.90	18.68	2.37	0.30	12.0	0.86	0.25
		b	48.2	1.13	0.72	45.32	1.43	0.66	6.2	1.13	0.77
	3a	a	64.0	1.35	0.90	18.68	2.37	0.30	12.0	0.86	0.25
		b	42.4	1.35	0.55	37.56	1.35	0.75	5.0	1.35	0.55

Four sets of the optical potentials listed in Table I were used. These were obtained from the global parametrization given in Refs. [38–42] and a χ^2 minimization analysis by means of the best fits to the experimental $d + {}^7$Li, $n + {}^9$Be, and $n + {}^{11}$B scattering angular distributions in the forward hemisphere at the corresponding projectile energies. This method for fitting provides an equally good reproduction of the experimental angular distribution within the main peak region, as will be shown below. As an illustration, for sets 2–4 of the optical potentials, Fig. 2(a) shows the results of comparison between the calculated angular distributions and the experimental data for elastic $d + {}^7$Li scattering taken from Ref. [39] (closed triangles) at most near corresponding energies. As is seen from this figure, the used sets reproduce well the corresponding experimental angular distributions up to ~90°. A similar result is obtained for set 1 of Table I. Besides, in Fig. 2(a), the result of calculation (dash-dotted line), obtained with the optical potentials for the set $S1$ recommended in Ref. [23], and its comparison with the experimental data [23] (open circle) are presented for the elastic $d + {}^7$Be scattering at $E_i = 4.5$ MeV. One can see that the optical potentials recommended in Ref. [23] describe well the experimental data only in the narrow angle range of the forward hemisphere. We note that the deuteron groups corresponding to the ground and first excited states were not resolved in the experiment. Moreover, a comparison of behavior of the experimental angular distributions of the elastic deuteron scattering on the nuclei ^{7}Be and ^{7}Li shows the overestimation of values of the elastic cross section in the angular range 55–75° in Ref. [23]. It may be the result of the underestimation of the cross section of the inelastic scattering with the formation of the 427-keV excitation level in ^{7}Be in the angle range mentioned above. Indeed, as can be seen from Fig. 5 of Ref. [39], at the elastic deuteron scattering on the nucleus ^{7}Li, the first minimum of the angular distribution is smoothly displaced towards small angles increasing the relative energy (approximately from 80° at 4 MeV to 70° at 5 MeV). The value of the differential cross section for the ^{7}Be(d,d_o)^{7}Be data at 4.5 MeV [23] changes by ~2.4 times between the scattering angles 60–75° (i.e., on the left slope of the expected first minimum of the angular distribution), still not reaching the minimum, whereas, at the same energy (from the data averaged on energy at 4 and 5 MeV [39]), the differential cross section for ^{7}Li(d,d_o)^{7}Li scattering changes only by

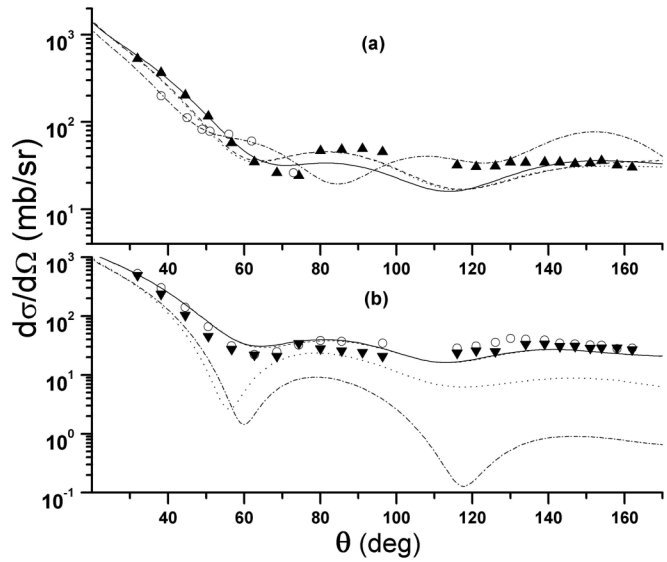

FIG. 2. Fit of the elastic $d + {}^7$Li and $d + {}^7$Be scattering cross sections by using different sets of optical potentials. In (a), the solid, dashed, and dotted lines correspond to sets 4, 3, and 2, whereas the dash-dotted line corresponds to set S1 from Ref. [23]; experimental data for the elastic $d + {}^7$Li scattering at $E_d = 6$ MeV (closed triangles) and for the $d + {}^7$Be scattering $E_d = 5.79$ MeV (open circles) are taken from Refs. [39] and [23], respectively. In (b), the solid and dashed lines correspond to sets 1a and 2a of the present work, and the dash-dotted and dotted lines correspond to sets 1 and 2 recommended in Ref. [22]; experimental data (open and close points) for the elastic $d + {}^7$Li scattering [39] at $E_d = 7.0$ and 8.0 MeV, respectively.

$\sim$1.3 times, reaching the first minimum at an angle $\sim 75^\circ$. It should be noticed that the position of the first minimum depends very smoothly on the mass number at the fixed energy (see, for example, Ref. [42]), and therefore the trend of the angular distribution and position of the first minimum for deuteron scattering on ^{7}Li and ^{7}Be nuclei should be similar. For specification of the cross section behavior in the region of the first minimum of angular distribution, which is an essential criterion for the realistic OMP selection, the experiment with a smaller energy dispersion of the ^{7}Be beam is needed. Taking into account the above-stated considerations, we do not include the OMPs recommended in Ref. [23] for the analysis of the ^{7}Be$(d,n)^8$B reaction performed below.

For calculation of the shell-model two-body bound-[^{8}B(^{7}Be $+p$) and $d(n+p)$] state wave functions the Woods-Saxon potential is used with varying the geometric parameters within the physically acceptable limit by means of adjusting the well depth to the experimental binding energy (0.137 MeV for the nucleus ^{8}B and 2.225 MeV for the deuteron d) for each of the geometric parameters. At first, we have tested the validity of the condition (6) for the first six experimental points of the angular distribution of the reaction presented in Ref. [23] and for all sets of the optical potentials of Table I. This test is done by changing the geometric parameters r_o and a of the Woods-Saxon potential, used for calculation of the bound-$(n+p)$ and (^{7}Be $+p$) state wave functions, in wide physically acceptable ranges ($r_o = 1.10$–1.40 fm and $a = 0.50$–0.75 fm) with respect to their "standard" values ($r_o = 1.25$ fm and $a = 0.65$ fm). Such variation of the r_o and a results in changing the single-particle ANCs ($b_{\mathrm{B};\,j_B} = b_{\mathrm{B};\,j_B}(r_o, a)$ and $b_{d;\,1/2} = b_{d;\,1/2}(r_o, a)$ [25]) with $j_B = 1/2$ and 3/2 within the intervals of $0.615 \leqslant b_{\mathrm{B};\,3/2} \leqslant 0.795$ fm$^{-1/2}$, $0.596 \leqslant b_{\mathrm{B};\,1/2} \leqslant 0.782$ fm$^{-1/2}$, and $0.900 \leqslant b_{d;\,1/2} \leqslant 0.984$ fm$^{-1/2}$.

Figure 3 shows a plot of the $\mathcal{R}_{3/2\ 1/2}(E_i,\theta;\, b_{B;3/2},b_{d;1/2})$ dependence only on the single-particle $b_{\mathrm{B};3/2}$ and the fixed value of $b_{d;\,1/2} = b_{d;\,1/2}(r_o,a) = 0.942$ fm$^{-1/2}$ at $r_0 = 1.3$ fm and $a = 0.65$ fm for the potential of the set 3 in Table I within the aforementioned interval for three angles θ ($\theta = 16.58^\circ$, 25.2°, and 34.23°) within the main peak. The width of the band for these curves is the result of the weak "residual" (r_o,a) dependence of $\mathcal{R}_{3/2\ 1/2}(E_i,\theta;\, b_{B;3/2},b_{d;1/2})$ on the parameters r_o and a (up to $\pm 1\%$) for $b_{\mathrm{B};3/2}(r_o,a) = \mathrm{const}$ [25]. The same dependence is also observed for $j_B = 1/2$ and other values of $b_{d;\,1/2}$. For example, the arithmetic averaged values of the $\mathcal{R}_{3/2\ 1/2}(E_i,\theta;\, b_{B;3/2},b_{d;1/2})$ and $\mathcal{R}_{1/2\ 1/2}(E_i,\theta;\, b_{B;1/2},b_{d;1/2})$ obtained in the intervals for $b_{B;\,j_B}$ ($j_B = 1/2$ and $3/2$) and $b_{d;\,1/2}$ mentioned above are equal to 63.31 ± 0.28 and 94.00 ± 0.64 mb fm/sr at $\theta = 16.58^\circ$ and equal to 35.93 ± 0.71 and 54.16 ± 0.91 mb fm/sr, respectively, at $\theta = 29.6^\circ$. Here, the pointed-out uncertainties are the averaged square errors, which involve those arising due to the observed weak dependence of these calculated functions with changing of $b_{B;\,j_B}$ and $b_{d;\,1/2}$ as well as the extremely weak "residual" (r_o,a) dependence of $\mathcal{R}_{3/2\ 1/2}(E_i,\theta;\, b_{B;\,j_B},b_{d;\,1/2})$ at $b_{B;\,j_B} = \mathrm{const}$ and $b_{d;\,1/2} = \mathrm{const}$. It is seen that at fixed values of θ within the main peak region the averaged values of the $\mathcal{R}_{j_B\ 1/2}(E_i,\theta;\, b_{B;\,j_B},b_{d;\,1/2})$ functions do not depend practically on the free parameters $b_{B;\,j_B}$ and $b_{d;\,1/2}$. Over these intervals for the free parameters the condition (6) is fulfilled within up to about $\pm 0.7\%$ for

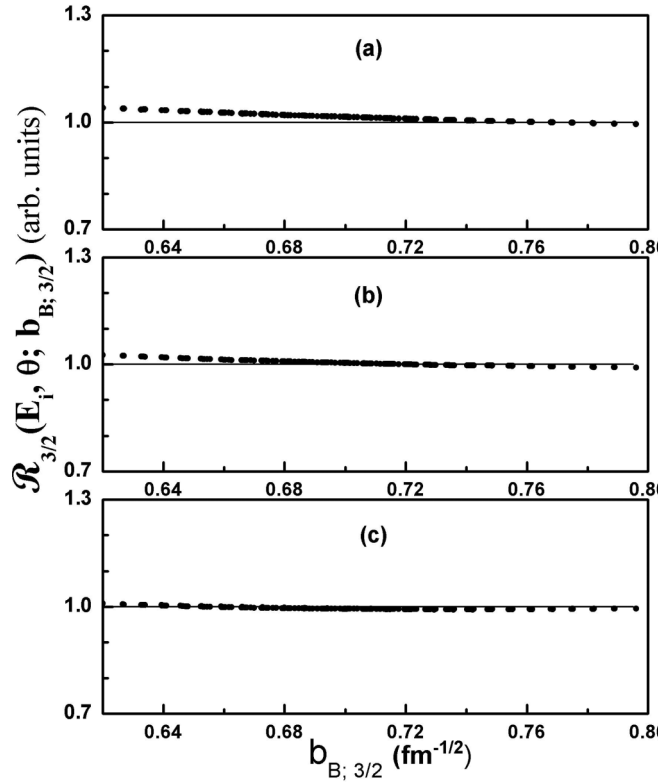

FIG. 3. The dependence of $\mathcal{R}_{3/2\ 1/2}(E_i,\theta;\, b_{B;3/2},b_{d;1/2})$ on the single-particle $b_{B;3/2}$ at $b_{d;1/2} = 0.942$ fm$^{-1/2}$ and the different angles θ for the energy of $E_i = 4.5$ MeV and with potential parameters of set 3 in Table I. In (a), (b), and (c), the calculated $\mathcal{R}_{3/2\ 1/2}(E_i,\theta;\, b_{B;3/2},b_{d;1/2})$ function is plotted for $\theta = 16.58^\circ, 25.2^\circ$, and 34.23°, respectively. The width of the bands for fixed values of $b_{B;3/2}$ corresponds to variation of the parameters r_o and a of the adopted Woods-Saxon potential within the intervals from $r_o = 1.10$ to 1.40 fm and $a = 0.50$ to 0.75 fm.

$j_B = 3/2$ and up to about $\pm 2.0\%$ for $j_B = 1/2$, whereas $\sigma^{\mathrm{DW}}_{l_d l_B}(E_i,\theta;\, b_{\mathrm{B};j_B},b_{d;1/2})$ entering (4) is a rapidly varying function of $b_{\mathrm{B};\,j_B}$ ($j_B = 1/2$ and $3/2$) and $b_{d;\,1/2}$. The same situation is observed for the other considered values of θ and the sets of the optical potentials from Table I.

We also performed calculations of the DWBA cross sections (3) at forward angles for different values of the cutoff radius R_{cut} [lower limit in radial integration over the distance (R) between centers of masses of the colliding particles] to check in an independent manner the peripheral character of the ^{7}Be$(d,n)^8$B reaction at the energy $E_i = 4.5$ MeV. Calculations have been done for all sets of the optical potentials of Table I and the Woods-Saxon potential for the bound state of ^{8}B with the standard geometric parameters ($r_o = 1.25$ fm and $a = 0.65$ fm) and the Thomas spin-orbital term. The dependence of the DWBA cross sections on the R_{cut}, $\frac{d\sigma}{d\Omega}(R_{\mathrm{cut}})$ is shown in Fig. 4(a) for set 3. It shows that the contribution of the region with $R \leqslant R_{\mathrm{cut}} \lesssim 5.0$ fm into the calculated DWBA cross section is strongly suppressed and makes from 1% up to 5% in the region of the main peak of the angular distribution, which does not exceed the experimental errors. The same result is obtained for sets 1, 2, and 4. The

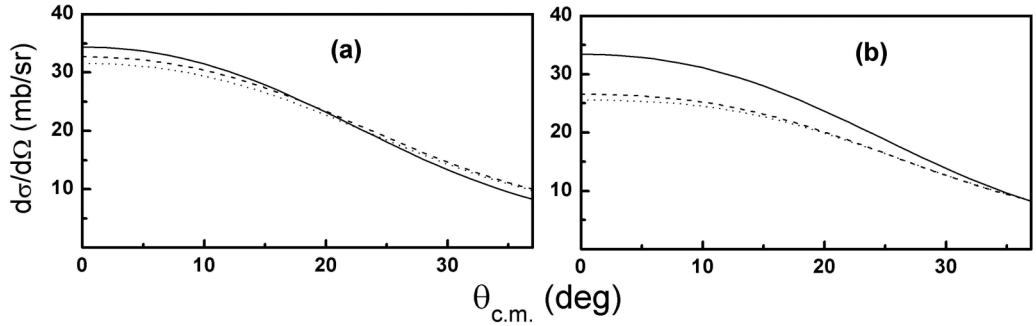

FIG. 4. Angular distributions depending on different cutoff radii ($R_{\rm cut}$) for $E_i = 4.5$ MeV (a) and $E_i = 5.8$ MeV (b) calculated in DWBA with potential parameters of sets 3 and 1a (Table I), respectively. The solid, dotted, and dashed lines are the differential cross sections calculated for the cutoff radius $R_{\rm cut} = 0.0$, 4.0, and 5.0 fm, respectively.

bound-state wave functions $r\varphi_{B;\,j_B}(r)$ ($j_B = 3/2$) of the ^{8}B nucleus in the (^{7}Be + p) channel calculated for different values of the geometric parameters reach their asymptotic behavior $b_{B,\,3/2}W_{-\eta_B;3/2}(2\kappa r)$ for $r \gtrsim 5.0$ fm, where $W_{-\eta_B;3/2}(x)$ is the Whittaker function, η_B is the Coulomb parameter for the ^{8}B = (^{7}Be + p) bound state, and $\kappa = \sqrt{2\mu_{p^7{\rm Be}}\varepsilon}$ in which ε is the binding energy of ^{8}B in (^{7}Be + p) channel. Figure 5 demonstrates the dependence of the bound-state wave function $r\varphi_{B;\,j_B}(r)$ ($j_B = 3/2$) on the geometric parameters r_o and a of the Woods-Saxon potential.

Testing condition (6) and calculating the DWBA cross sections (3) at the first four experimental points of the angular distribution also were done for different values of the cutoff radius $R_{\rm cut}$ for the ^{7}Be(d,n)^{8}B reaction at the energy $E_i = 5.8$ MeV [22]. The calculations were performed for the sets 1a, 2a, and 3a of the optical potentials obtained by fitting the experimental scattering data closest to the kinematics of Ref. [22] in the same way as done above. The results

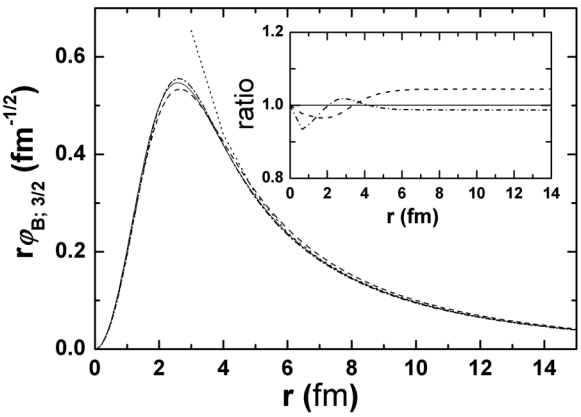

FIG. 5. The radial behavior of the single-particle ^{8}B[= (^{7}Be + p)] bound-state wave function $r\varphi_{B;\,j_B}(r)$ with $j_B = 3/2$ calculated for the Woods-Saxon potential with different sets of (r_o, a) pairs and $b_{B,\,3/2}$: (1.00 fm; 0.50 fm) and 0.6200 fm$^{-1/2}$ (the dashed line), (1.25 fm; 0.65 fm) and 0.7679 fm$^{-1/2}$ (the solid line), and (1.40 fm; 0.80 fm) and 0.7960 fm$^{-1/2}$ (the dashed-dotted line). The Coulomb radius $r_C = 1.30$ fm. The dotted line is the tail $b_{B,\,3/2}W_{-\eta_B;3/2}(2\kappa r)$ of the bound-state wave function $r\varphi_{l_B\,j_B}(r)$ with $b_{B,\,3/2} = 0.7679$ fm$^{-1/2}$ ($r_o = 1.25$ fm and $a = 0.65$ fm).

are presented in Table I. Figure 2(b) shows the results of comparison of the angular distributions calculated for sets 1a and 2a (solid and dashed lines, respectively) with the experimental data for elastic $d + {}^7$Li scattering taken from Ref. [39] (open circles and closed triangles for $E_d = 7.0$ and 8.0 MeV, respectively). As seen from the figure, the used sets reproduce well the corresponding experimental angular distributions up to ~90°, whereas the optical potentials recommended in Ref. [22] provide poor fits to the experimental data [see dash-dotted and dotted lines in Fig. 2(b)]. The same situation is observed for set 3a. But the calculations performed for all of the considered sets of the optical potentials show that the condition (6) is fulfilled within from ±10% up to ±14% relative the central values of $\mathcal{R}_{j_B\,1/2}(E_i,\theta;\, b_{B;\,j_B},b_{d;\,1/2})$ functions over the above-mentioned intervals for $b_{{\rm B};\,3/2}$ and $b_{{\rm B};\,1/2}$ for each angle θ inside the main peak region. The same situation was observed in Ref. [27] where the optical potentials from Ref. [22] were used. The dependence of the DWBA cross sections on $R_{\rm cut}$ at the forward angles is shown in Fig. 4(b) for set 1a. As is seen from the figure, the contribution of the region with $R \leqslant R_{\rm cut} \lesssim 5.0$ fm to the calculated DWBA cross section is noticeable and occurs to be from 17% up to 23% in the region of the main peak of the angular distribution. The same result is obtained for the sets 2a and 3a.

It follows from here that the ^{7}Be(d,n)^{8}B reaction at the energy $E_i = 5.8$ MeV is not purely peripheral due to the fact that the contribution of the interior part of the matrix element into the $\mathcal{R}_{j_B\,1/2}(E_i,\theta;\, b_{B;\,j_B},b_{d;\,1/2})$ function is significant. One notes once more that the strong dependence of this function on $b_{B;\,j_B}$ and $b_{d;\,1/2}$ is associated mainly with the interior part of the matrix element and is determined by the bound state $\varphi_{B;\,j_B}(r;\, b_{B;\,j_B})$ and $\varphi_{d;\,1/2}(r;\, b_{d;\,1/2})$ wave functions. For illustration, we present in Fig. 5 the changing of the $\varphi_{B;\,j_B}(r;\, b_{B;\,3/2})$ wave function for three fixed values of $b_{B;\,3/2}$ ($b_{B;\,3/2} = 0.620$; 0.768 and 0.796 fm$^{-1/2}$). For these values of $b_{B;\,3/2}$ the calculated wave functions change noticeably in the interior region, whereas the observed discrepancy grows from 3 to 8% as the relative distance between the "valence" proton and the center mass of the core (^{7}Be) decreases from 3.0 to 0.2 fm (see the insert in Fig. 5).

Therefore, in reality, one should take into account the effect of a node at short distance in the bound-state wave function which is due to Pauli antisymmetrization. Besides,

as mentioned above, the additional difficulty, connected with uncertainties of the optical model potentials in the interior part of the matrix element for description of the elastic scattering of lightest particles on light nuclei [25,37,43] can be faced. The facts mentioned above can apparently be one of the reasons why the value of the spectroscopic factor for ^{8}B in the (^{7}Be + p) configuration, extracted in Ref. [24] from the ^{7}Be(d,n)^{8}B analysis at the energy $E_i = 5.8$ MeV with using different sets of the input data, has a large spread (about 30%). Therefore, the analysis of the experimental data of Ref. [22] performed within the modified DWBA in Ref. [27] and in the present work as well as that performed in Ref. [24] cannot allow one to obtain the reliable ANC values. In contrast to this case, the ^{7}Be(d,n)^{8}B reaction at the energy $E_i = 4.5$ MeV is predominantly peripheral in the main peak region of the angular distribution. At this case, the influence of the effects connected with the true structure of many-particle wave functions of the nuclei (deuteron, ^{7}Be, and ^{8}B), exhibited mainly in the interior part of the matrix element, can be ignored. So, in the surface and outer regions of the nucleus, the wave functions of the relative motion at the initial and final states can be described by the optical model, and the bound- [(^{7}Be + p)] state wave function by the one-particle shell-model wave function reducing their uncertainties to a minimum. Consequently, the experimental data of Ref. [23] are used for obtaining the "indirectly determined" values of the ANCs for ^{7}Be + $p \rightarrow {}^8$B.

The condition (7) was used for each θ from the main peak region of the angular distribution as only in such a case is the absolute value of the differential cross section defined by the ANC. For illustration, we present in Fig. 6 the results of calculation of the ratio in the right-hand side of the expression (7), where instead of the calculated differential cross section the corresponding experimental cross sections are taken. The calculations were performed for $\theta = 16.6^\circ$ and 29.6° and the sets 2 and 3 of the optical potentials. Here, it was taken into account the fact that the ratio $\tilde{R} = b_{B;1/2}(r_o, a)/b_{B;3/2}(r_o, a)$ practically does not depend on variation of the free r_o and a parameters of the Woods-Saxon potential (r_o ranging from 1.10–1.40 fm and a in the range of 0.50–0.75 fm). The value of $\tilde{R}$ is equal to 0.9742 ± 0.0065. It is seen from the figure that the C_B^2 values are weakly dependent on the $b_{B;3/2}$ value. However, the values of the spectroscopic factor Z_B determined by the relation $Z_B = 1.006 C_B^2/b_{B;3/2}^2$, which can be obtained from (5) with use of the aforementioned values for $\tilde{R}$ and λ, change strongly [Fig. 6(a)]. We found that the same dependencies for C_B^2 and Z_B occur for all other considered scattering angles and the sets of the optical potentials from Table I.

To increase the accuracy of the ANC values required for their astrophysical application, the contribution of the compound (^{9}B*) nucleus (CN), the d-component of the bound -state wave functions of deuteron, the remnant $V_{n\mathrm{Be}}^N - V_f^N$ in the first term in the right-hand side of Eq. (2), and coupled-channel effects (CCE) connected with the elastic and inelastic $d + {}^7$Be scattering should be taken into account. The CN and CCE contribution were calculated as in Refs. [22,23] and Refs. [44,45], respectively, whereas the estimation of contribution of the remnant $V_{n\mathrm{Be}}^N - V_f^N$ was done by using the FRESCO code [46].

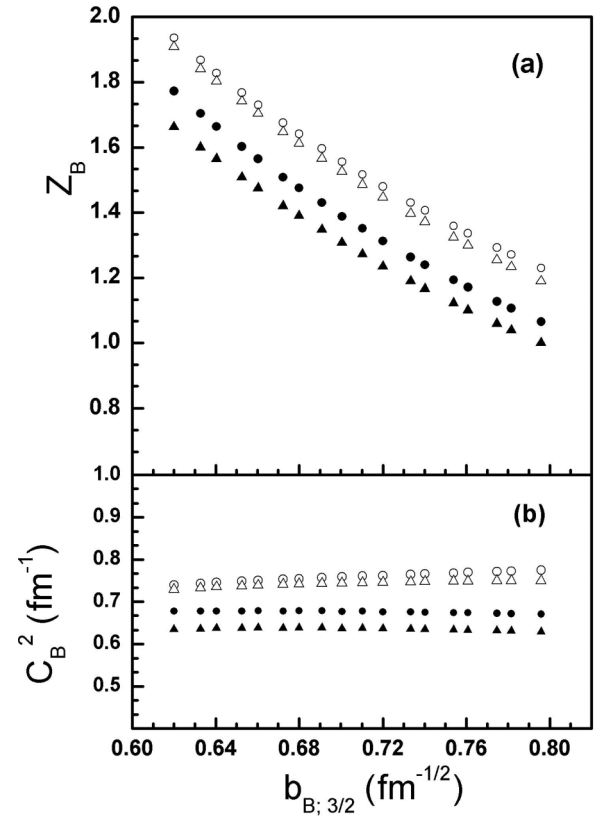

FIG. 6. Values of the spectroscopic factors Z_B (a) and the squared ANC C_B^2 (b) as a function of the single-particle $b_{B;3/2}$ obtained using the modified DWBA ^{7}Be(d,n)^{8}B analysis at the energy $E_i = 4.5$ MeV and $b_{d,\,1/2} = 0.942$ fm$^{-1/2}$ for the different fixed angles θ and the sets of the optical potentials. Data denoted by ○ and △ (● and ▲) correspond to the experimental points θ of 16.6° and 29.6°, respectively, for set 3(2).

Influence of the CN contribution Δ_{CN} on the ANC values extracted for each θ from the main peak region has been determined using the results of work [23], where $\Delta_{\mathrm{CN}} = 2|d\sigma_{\mathrm{CN}}/d\Omega - d\sigma/d\Omega|/(d\sigma_{\mathrm{CN}}d\Omega + d\sigma/d\Omega)$ in which $d\sigma_{\mathrm{CN}}/d\Omega$ is the CN cross section. The contribution of Δ_{CN} increases with increase of θ in the main peak region, which leads to a decrease of the ANC values, obtained from the relation (7). For example, it is by 0.8% at $\theta = 8.2^\circ$ and by 2.9% at $\theta = 34.2^\circ$ for set 1 and by 1.0% at $\theta = 8.2^\circ$ and by 3.1% at $\theta = 34.2^\circ$ for set 3. The same results practically occur for other sets of the used optical potentials. As a whole, the CN contribution to the cross sections [23] in the main peak region is quite small and, consequently, it results in barely changing the extracted ANC values. As for the contribution of the d-component of the bound-state wave functions for the deuteron to the calculated single-particle cross section, the calculation shows that this contribution within the main peak region is negligibly small since it changes the ANC values extracted from the main peak region only within 0.2–0.3%.

The influence of the $V_{n\mathrm{Be}}^N - V_f^N$ remnant on the ANC values obtained without taking into account this remnant was estimated. However, so far as is known to us, at the energy of the neutron corresponding to the kinematic of the

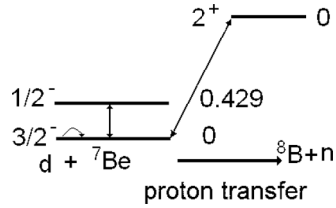

FIG. 7. The coupling scheme used in calculations of the cross section for the ^{7}Be(d,n)^{7}Be reaction by the coupled reaction channels method.

considered reaction, there are no data for the n^7Be and n^7Li scatterings. Therefore, for the core-core interaction ($V^N_{n\mathrm{Be}}$) entering the four-ray vertex of the diagram Fig. 1(b), the optical potentials adopted for the exit channel of the analyzed reaction are used, as in Ref. [24]. The result shows that taking into account the $V^N_{n\mathrm{Be}} - V^N_f$ remnant changes the ANC values within 1%–5% with respect to those obtained without taking into account the remnant for six considered angles θ from the region of the main peak. This result is apparently not accidental and can be explained by the fact that the peripheral reaction at $E_i = 4.5$ MeV is first governed by the nearest to the physical ($-1 \leqslant \cos\theta \leqslant 1$) region singularity at $\cos\theta = \xi$ of the reaction amplitude [47]. Second, the dominant role played by the singularity $\cos\theta = \xi$ is the result of the peripheral nature of the considered reaction at least near the main peak of the angular distribution. For an illustration of this fact, the calculated singularities [48] of the reaction amplitude at $E_i = 4.5$ MeV corresponding to the pole and triangle diagrams plotted in Figs. 1(a) and 1(b) are located at $\cos\theta = \xi = 1.29$ and $\cos\theta = \xi_\Delta = -7.71$, respectively. Study of the analytical properties of the amplitudes connected with the second term in V^{TB} over the variable $\cos\theta$ [48] shows that their singularities are located essentially farther from the right and left boundaries of the physical region for $\cos\theta$ than those of ξ and ξ_Δ, respectively. It is seen from here that the singularities of the amplitudes corresponding to the triangle diagram Fig. 1(b) and the types of diagram plotted in Fig. 1(c) are located far from the physical region of changing the variable $\cos\theta$ within the main peak, whereas the singularity at $\cos\theta = \xi$ is nearest to the right part ($\cos\theta = 1$) of the boundary of the physical region $-1 \leqslant \cos\theta \leqslant 1$ and, therefore, it must namely determine both the behavior of the cross section and its absolute value in the main peak.

The CCE contributions to the DWBA cross sections for each experimental point of θ from the main peak region has been determined using the FRESCO computational code [46], similarly as in Ref. [44]. The coupling between the ground ($E^* = 0.0$; $J^\pi = 3/2^-$) and first excited ($E^* = 0.429$ MeV; $J^\pi = 1/2^-$) states of the ^{7}Be nucleus was calculated with the collective form factor of the rotational model for the quadrupole transition, as in Ref. [45] (see the coupling scheme in Fig. 7). The spectroscopic amplitudes A_j are taken from Ref. [22] ($A_j = Z_j^{1/2}$). As mentioned above, the optical potentials adopted for the exit channel are used for the core-core interaction. The deformation length δ_2 is taken equal to 2.0 fm, which results in a change of the deformation parameter $\delta_2 (= \beta_2 R_{\mathrm{Be}}$, where $R_{\mathrm{Be}} = r_o 7^{1/3})$ from 1.02 to 1.04 depending on the parameter radius r_o for the real parts of the used optical potentials. The averaged value of the β_2 is equal to 1.03, which is in a good agreement with the value of 1.00 obtained in Ref. [49] from the analysis of $\alpha + ^7$Li scattering. The results are presented in Table II for all sets of the used optical potentials. The coupled-channel differential cross sections and the ratio Δ_{CCE} of the differential cross section calculated without the CCE contribution to that calculated with the CCE contribution are given in the forward hemisphere. As seen from Table II, for all used sets of the optical parameters the effect of contribution of the CCE on the calculated cross section increases as the scattering angle increases, which results in changing the extracted ANC values from 0.6% to 5%.

TABLE II. Coupling channel effects for the ^{7}Be(d,n)^{8}B reaction at $E_i = 4.5$ MeV in the forward hemisphere calculated for each set of the optical potential used. Differential cross sections are given in mb/sr. Figures in brackets are the ratio Δ_{CCE} of the differential cross section calculated without the CCE contribution to that calculated with the CCE contribution.

θ	$d\sigma_{\mathrm{CCE}}/d\Omega(\Delta_{\mathrm{CCE}})$			
(deg.)	Set 1	Set 2	Set 3	Set 4
1.00	47.6(1.029)	49.7(0.977)	49.0(1.017)	50.8(1.057)
8.20	45.4(1.026)	47.3(0.974)	46.6(0.965)	48.2(1.052)
16.60	38.4(1.047)	39.8(0.964)	38.9(0.960)	39.9(1.038)
20.90	33.4(1.006)	34.3(0.968)	33.3(0.956)	34.0(1.027)
25.20	27.8(0.996)	28.3(0.958)	27.2(0.951)	27.6(1.014)
29.60	22.1(0.983)	22.3(0.951)	21.2(0.944)	21.3(0.995)
34.20	16.7(0.967)	16.8(0.941)	15.7(0.935)	15.6(0.969)

Thus, the detailed study of the peripheral character of the considered reaction makes it possible to extract the values of ANCs $C^2_{B;3/2}$ and $C^2_B [= C^2_{B;3/2}(1+\lambda)]$ by using the experimental differential cross sections and values of the function $\mathcal{R}_{j_B}$ in the right-hand side of the relation (7) for the different scattering angles from the forward hemisphere. At this, to improve an accuracy of the extracted ANC values, the contribution of the compound nucleus, the $V^N_{n\mathrm{Be}} - V^N_j$ remnant, and the CCE should be taken into account.

The squared ANC C^2_B for $^7\mathrm{Be} + p \to {}^8\mathrm{B}$ obtained for each experimental θ point, corresponding to the sets 1–4, are presented in Figs. 8(a)–8(d), respectively. The uncertainties pointed out in this figure correspond to the averaged square errors found from Eq. (7), which includes both the experimental errors in the $d\sigma^{\mathrm{exp}}/d\Omega$ and the above-mentioned uncertainty of the ANC for $p + n \to d$ (experimental parts) as well as the mentioned uncertainties in the $\mathcal{R}_j(E_i,\theta;\, b_{B;\,j})$ functions. The solid line and the width of the band present the results for the weighted mean values and their uncertainties [50], respectively. It is seen from Fig. 8 that the right-hand side of relation (7) practically does not depend on the angle θ although absolute values of the experimental cross sections depend noticeably on the angle θ and change by up to the factor 2.6 with θ changing from 8.2° to 34.2°.

The weighted means and their uncertainties for the squared ANCs derived for each set of the optical potential are presented in lines 1–8 of Table III. There the first figures in brackets are experimental uncertainties, which are derived from the

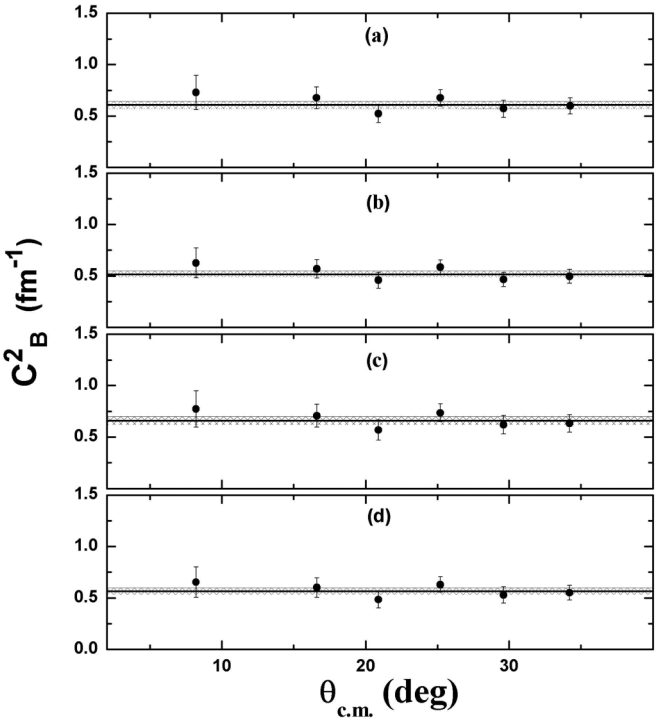

FIG. 8. The values of the squared ANC C_B^2 for $^7\mathrm{Be}+p \to {}^8\mathrm{B}$ for each of the experimental θ. Data in (a)–(d) are obtained from the analysis of the experimental differential cross sections of Refs. [23] at $E_i = 4.5$ MeV and sets 1–4 of the optical potentials, respectively. The solid lines present the results for the weighted mean values. The widths of the bands are the corresponding weighed uncertainties.

averaged square errors of the above-mentioned experimental parts for each point θ in Fig. 8. The second figures in brackets are theoretical uncertainties associated with the uncertainties in the $\mathcal{R}_j(E_i,\theta;\, b_{B;\,j})$ functions for each point θ in Fig. 8. In the second, third, and fourth columns of this table, the results obtained with taking into account the CN [but without the remnant $V^N_{n\mathrm{Be}} - V^N_f$ terms (RT)], RT, and CCE contributions are given, respectively. The RT and CCE contributions on the ANC values, as seen in Table III, change the ANC values from 3.1% to 6.8% and from 0.6% to 4.6%, respectively, with respect to each other in dependence of a set of the optical parameters, which do not exceed the experimental errors for the $d\sigma^{\mathrm{exp}}/d\Omega$ [23]. The final averaged values of the squared ANCs derived from the ANCs given in lines 1–8 of Table III are also presented in the 9th and 10th lines of Table III. As is seen from Table III, the RT and CCE contributions change the final ANC values about 0.5% and 1.5%, respectively.

The ANC value recommended in the present work is $C_B^2 = 0.613 \pm 0.030\,(\mathrm{exp}) \pm 0.052(\mathrm{th})$ fm^{-1} or $C_B^2 = 0.613 \pm 0.060$ fm^{-1} with the overall uncertainty, which are also listed in the second and third lines of Table IV together with those obtained by the other authors in Refs. [10,13,16,20,24,51–54]. The overall uncertainty for the recommended ANCs is about 10%. As is seen in Table IV, the weighted mean of C_B^2, obtained in the present work, is in excellent agreement with that of Ref. [10], which was derived from the independent analysis of the experimental $^7\mathrm{Be}(p,\gamma)^8\mathrm{B}$ astrophysical S factors at extremely low energies. However, the obtained value for C_B^2 differs noticeably from that recommended in Refs. [16,24,51,52]. As we discussed above, the ANC value of Ref. [16] is model dependent [9,19,20,55] on account of using the first order over the ΔV_f^C potential. The ANC value of Ref. [24] and the discussed theoretical uncertainty of it, which can easily be obtained using the $S_{17}(0)$ value derived in Ref. [24] (see Table IV) and its relation with the ANC given there, is also model dependent because of the fairly large ambiguity for the spectroscopic factors. The results of Refs. [51,52] were obtained from the $^7\mathrm{Be}(p,\gamma)^8\mathrm{B}$ R-matrix analysis, where the direct part of the amplitude is expressed in terms of the channel reduced width and is also determined in a model-dependent way. In reality, the ANC obtained in Refs. [51,52] can have the uncertainty arising due to an ambiguity in values determined by fitting all the other free parameters used. In addition, as seen in Table IV, the ANCs obtained by us also differ noticeably from the values of C_B^2 derived in Refs. [20,53] from the $^{208}\mathrm{Pb}(^8\mathrm{B},p^7\mathrm{Be})^{208}\mathrm{Pb}$ breakup reaction. In Ref. [20], this process is analyzed, as noted above, within the strict three-body model based on the CDCCM in which all nuclear and Coulomb interactions are

TABLE III. The weighted mean values of the squared ANCs for $^7\mathrm{Be}+p \to {}^8\mathrm{B}$ obtained without and with the $V^N_{n\mathrm{Be}} - V^N_f$ remnant terms (RT) as well as with the CCE contribution for each of the sets 1–4 of the optical potentials at $E_i = 4.5$ MeV. Figures in brackets are experimental and theoretical uncertainty, respectively. The values in the even lines correspond to the ANC values with $j_B = 3/2$.

	C_B^2, $C^2_{B;3/2}$ fm^{-1}		
Set	Without RT	With RT	With CCE
1	0.598(±0.037; ±0.034)	0.623(±0.038; ±0.034)	0.627(±0.038; ±0.038)
	0.525(±0.032; ±0.030)	0.545(±0.033; ±0.030)	0.549(±0.033; ±0.030)
2	0.596(±0.034; ±0.029)	0.575(±0.033; ±0.028)	0.555(±0.032; ±0.028)
	0.521(±0.030; ±0.025)	0.503(±0.029; ±0.025)	0.486(±0.028; ±0.025)
3	0.705(±0.041; ±0.030)	0.727(±0.042; ±0.031)	0.694(±0.040; ±0.032)
	0.617(±0.036; ±0.026)	0.636(±0.037; ±0.027)	0.607(±0.035; ±0.028)
4	0.609(±0.037; ±0.023)	0.569(±0.034; ±0.021)	0.582(±0.035; ±0.024)
	0.533(±0.032; ±0.020)	0.498(±0.030; ±0.018)	0.509(±0.031; ±0.021)
Averaged	0.625(±0.037; ±0.039)	0.622(±0.037; ±0.046)	0.613(±0.030; ±0.052)
Mean	0.547(±0.032; ±0.034)	0.544(±0.032; ±0.040)	0.536(±0.026; ±0.046)

exactly taken into account in the all-order perturbation theory in the transition operator. Nevertheless, first, the cross section of the considered breakup process is expressed in terms of the spectroscopic factor Z_B (denoted by α in Ref. [20]), which is really model dependent. Second, in Ref. [20], the dependence on channel spin is ignored in the effective p-^{7}Be interaction for the single-particle wave function of ^{8}B and the overestimated value of λ (= 0.159) was used (see above and Refs. [16,36]). Therefore, under such assumptions, the Z_B extracted in Ref. [20], which was used in Eq. (5) together with the single-particle ANC for the adopted potential, becomes strongly model dependent. For example, the values of $\omega_I = \sqrt{Z_{B;I}/Z_B}$, in terms of which the calculated single-particle cross section (σ) is parameterized (see Eq. (45) in Ref. [20]), are taken equal to 0.397 and 0.918 for $I = 1$ and 2, respectively, where I is a channel spin. But they are equal to 0.497 and 0.868 for $I = 1$ and 2 for Barker's spectroscopic factors ($Z_{B;I=1} = 0.251$ and $Z_{B;I=2} = 0.765$) [56]. Apparently, all these facts are the possible reasons why the ANC derived in Ref. [20] is underestimated in comparison with that obtained in the present work. In Ref. [53], the consideration is restricted only by the Coulomb interactions in the first-order perturbation theory in the transition operator. However, as demonstrated in Ref. [24], this assumption is not correct and leads to the underestimated value of the ANC obtained. Besides, in Ref. [53], the three-body Coulomb postdecay acceleration effects in the final state of the Coulomb breakup reaction is not taken into account. As shown quantitatively in Ref. [57], the influence of these effects grows as the relative kinetic energy E of the breakup fragments decreases, especially at extremely low energies. But our result for ANC obtained for $j_B = 3/2$ is in good agreement with that of Ref. [54] derived from the ^{58}Ni(^{8}B , p^7Be)^{58}Ni analysis for the $1p_{3/2}$ proton orbital in ^{8}B. Besides, the result of Ref. [13], obtained within the three-body microscopic approach for the Minnesota (MN) form of the NN potential, is also in a good agreement with that of the present work. It follows from here that the microscopic three-body (α^3He p) cluster calculation performed in Ref. [13] for MN potential correctly reproduces the normalization of the tail of the radial overlap function of the ^{8}B in the (^{7}Be $+p$) channel.

The weighted means for C_B^2 presented in Table III for sets 1–4 of the optical potentials and the corresponding averaged values of the $\mathcal{R}_{j_B}(E_i,\theta;\, b_{B;\,j_B})$ functions were used in the expressions (3) and (4) for calculating the differential cross sections for the ^{7}Be(d,n)^{8}B reaction at $E_i = 4.5$ MeV. The results of calculations and their comparison with the experimental data [23] are displayed in Fig. 9. As seen from this figure, the calculated cross section is in a good agreement with the experimental data in the main peak region of the angular distribution for all sets of the optical potentials.

III. APPLICATION FOR THE NUCLEAR ASTROPHYSICAL REACTION AND THE EFFECTIVE-RANGE EXPANSION

A. $S_{17}(E)$ for ^{7}Be(p,γ)^{8}B reaction at solar energies

The ANC value for $p + {}^7\text{Be} \to {}^8\text{B}$ presented in the last line of Table III was used for calculation of the astrophysical S factor of the ^{7}Be(p,γ)^{8}B reaction at zero energy by using the formula [15]

$$S_{17}(0) = 37.26 C_B^2 \ (\text{eV b}). \tag{8}$$

The obtained value of $S_{17}(0)$ is presented in Table IV along with the results obtained within the other methods by other authors. As is seen from Table IV, the $S_{17}(0)$ value obtained in the present work is in a good agreement with that of Ref. [10] and of Ref. [13] obtained for the MN potential as well as with $S_{17}(0) = 23.27$ eV b, which can be obtained from the interpolating formula $S_{17}(E) = 23.27–40.53E + 327.30E^2$ derived by us from the polynomial formula (43) of Ref. [58] for Barker's potential and the above-mentioned values of the spectroscopic factors [56]. At the same time, our result differ from those of Refs. [16,20,21,23,24,51,52,55]. The following should be noted. In Refs. [16,20,23,24,51,52] the value $S_{17}(0)$ was obtained by using the underestimated value of the ANC in respect to that derived in the present work. In Ref. [20], to obtain the value of $S_{17}(0)$ the relation between $S_{17}(0)/C_B^2$ and the s-wave ^{7}Be $+ p$ scattering length [59] (see also below) was used, in which the scattering lengths for $I = 1$ and 2 were calculated with the Barker's potential. The ANCs were extracted there by using another form of the p-^{7}Be potential by ignoring its I dependence, and, therefore, these calculations were not self-consistent. In Refs. [21,55], for obtaining the $S_{17}(0)$ value, the procedure of the artificial fitting the highly precise experimental data measured there to the astrophysical S factors calculated in Ref. [13] was applied. Therefore, the results of Refs. [21,55] obtained for $S_{17}(0)$ are model dependent since the results of Ref. [13] presented also in Table IV appreciably depend on the form of the used NN potentials. The result of the solar fusion II [8], which was compiled also from the results of Refs. [21,55], differs also noticeably from that obtained in the present work. Besides, as seen from Table IV, there is the discrepancy between our result for $S_{17}(0)$ and those of Refs. [53,60–63] obtained from the ^{8}B Coulomb breakup analysis. Apparently, one of the possible reasons of this discrepancy is the fact that, in Refs. [53,60–63], first order over $\Delta V_f^{(C)}$ is used in the transition operator [20] and the above-mentioned three-body Coulomb postdecay acceleration effects in the final state [57] are not taken into account. Nevertheless, our result for $S_{17}(0)$ obtained only with taking into account the value of ANC for $j_B = 3/2$, which is equal to 20.0 ± 2.0 eV b, is in excellent agreement with the result of Ref. [54]. The latter has also been obtained with taking into account only the $1p_{3/2}$ orbital proton contribution in the ^{8}B nucleus.

The results of extrapolation of the astrophysical S factors at extremely low energies, including close to the Gamov peak, $S_{17}(20$ keV), $S_{17}(50$ keV), and $S_{17}(120$ keV), which can be obtained within the MTBPA [15] by using the ANC values of the present work, are equal to 22.0 ± 2.5, 21.2 ± 2.5, and 20.4 ± 2.0 eV b, respectively.

We note that the ratio $S_{17}(E)/S_{17}(0)$ obtained from the results of the present work is equal to 0.97, 0.93, and 0.89 at $E = 20$, 50, and 120 keV, respectively. The same results for the ratio can be obtained using the rational expression proposed in Ref. [64]. It follows from here that the ratio $S_{17}(E)/S_{17}(0)$ obtained using the results of the present work and that of

TABLE IV. The squared ANC ($C_B^2 = C_{B;1/2}^2 + C_{B;3/2}^2$) for $^7\mathrm{Be} + p \rightarrow {}^8\mathrm{B}$ and the astrophysical S factor [$S_{17}(0)$] for the direct radiative capture $^7\mathrm{Be}(p,\gamma)^8\mathrm{B}$ reaction.

Method	C_B^2 (fm^{-1})	$S_{17}(0)$ (eV b)	Refs.
MDWBA			The
$^7\mathrm{Be}(d,n)^8\mathrm{B}$	0.613 ± 0.030 (th) $\pm$ 0.052(exp)	22.8 ± 1.1 (exp) $\pm$ 1.9(th)	present
	0.613 ± 0.060[a]	22.8 ± 2.2[a]	work
MTBPA			
$^7\mathrm{Be}(p,\gamma)^8\mathrm{B}$	0.628 ± 0.017	23.40 ± 0.63	[10]
MDWBA			
$^{10}\mathrm{B}(^7\mathrm{Be},{}^8\mathrm{B})^9\mathrm{Be}$			
$^{14}\mathrm{N}(^7\mathrm{Be},{}^8\mathrm{B})^{13}\mathrm{C}$	0.465 ± 0.041	18.2 ± 1.8	[16]
Breakup			
$^{208}\mathrm{Pb}(^8\mathrm{B},p^7\mathrm{Be})^{208}\mathrm{Pb}$	0.548	$21.7^{+0.37}_{-0.24}$ (th) $\pm$ 0.50(exp)	[20]
CDCCM			
$^7\mathrm{Be}(d,n)^8\mathrm{B}$	$0.545^{+0.036}_{-0.034}$ (th) $\pm$ 0.070(exp)	$20.96^{+1.4}_{-1.3}$ (th) $\pm$ 2.7(exp)	[24]
R-matrix			
$^7\mathrm{Be}(p,\gamma)^8\mathrm{B}$	0.518[b]	19.4[b]	[51]
	0.491	17.3 ± 3.0	[52]
Coulomb breakup			
A($^8\mathrm{B},p^7\mathrm{Be}$)A	0.450 ± 0.072	17.4 ± 1.5	[53]
$^{58}\mathrm{Ni}(^8\mathrm{B},p^7\mathrm{Be})^{58}\mathrm{Ni}$	0.547 ± 0.027[b]	20.8 ± 1.1[b]	[54]
Microscopic three-	0.812	29.45[c]	[13]
body ($\alpha^3\mathrm{He}\ p$) model	0.668	24.65[d]	[13]
CDCCM DWBA			
$^7\mathrm{Be}(d,n)^8\mathrm{B}$		20.7 ± 2.4	[23]
Phenomenological		21.2 ± 0.7	[55]
way		21.4 ± 0.6 (th) $\pm$ 0.5(exp)	[21]
Coulomb breakup			
$^{208}\mathrm{Pb}(^8\mathrm{B},p^7\mathrm{Be})^{208}\mathrm{Pb}$		20.6 ± 1.2[e]± 1.0[f]	[60]
		18.6 ± 1.2[e]± 1.0[f]	[61,62]
		20.6 ± 0.8[g]± 1.2[h]	[63]
Solar fusion II		20.8 ± 0.7[e]± 1.4[f]	[8]

[a]The overall uncertainty.
[b]For the $p_{3/2}$ state.
[c]The V2 potential.
[d]The MN potential.
[e]The exp. error.
[f]The th. error.
[g]The stat. error.
[h]The sys. error.

Ref. [64] reproduce correctly the energy dependence of the $S_{17}(E)$ at solar energies ($E \lesssim 120$ keV).

Thus, the C_B^2 value and the values of $S_{17}(E)$ at the solar energies ($E = 0$, 20, and 50 keV) derived in the present work with the uncertainty about 10% confirm the independent results of Ref. [10] obtained with the uncertainty about 3%. Therefore, these can be considered as the "best" values obtained by the indirect method so far. The $S_{17}(E)$ obtained in the present work and in Ref. [10] could also be used as the main input data in Eq. (1) for the correct estimation of the solar neutrino flux [1,8]. Nevertheless, more precise data are needed for such an estimation of the boron neutrino flux. As shown in our paper, the experimental errors dominate in the ANC values extracted from analysis of the $^7\mathrm{Be}(d,n)^8\mathrm{B}$ reaction at 4.5 MeV (center of mass). Moreover, this reaction becomes less peripheral at the larger energies. So, it would be expedient to carry out new precise measurements of the $^7\mathrm{Be}(d,n)^8\mathrm{B}$ reaction and the $d + {}^7\mathrm{Be}$ scattering at other near-barrier energies of radioactive ^{7}Be [less than 4.5 MeV (center of mass)] and as close to forward-scattering angles as possible.

B. s-wave $p + {}^7$Be scattering length and the slope of $S_{17}(0)$

It is now of interest to apply the ANCs and $S_{17}(0)$ derived by us above for obtaining information about experimental values of the s-wave $p + {}^7\mathrm{Be}$ scattering length $a_o^{(I)}$ and their average one $\bar{a}_o$ [59] ($I = 1$ and 2). To this end, we determine the squared ANC values in other spin

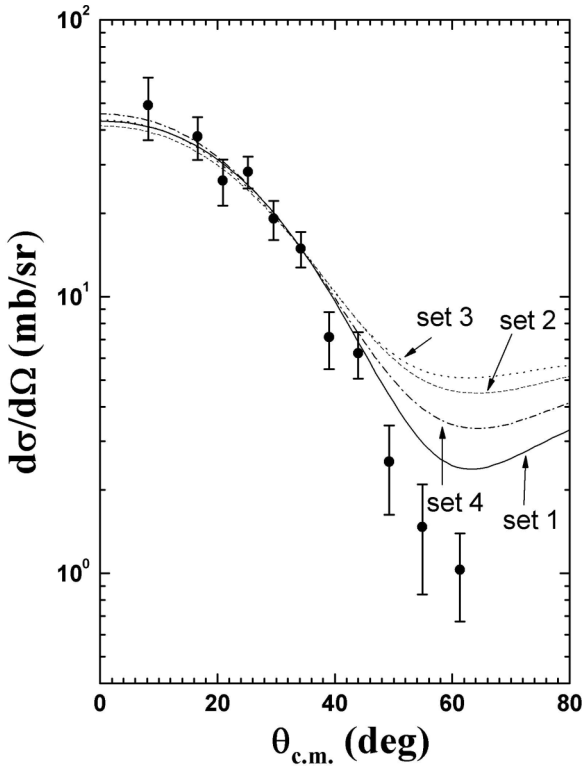

FIG. 9. Angular distribution of the differential cross section for the ^{7}Be$(d,n)^8$B reaction at $E_i = 4.5$ MeV together with the theoretical calculations performed for the different sets of the optical parameters from Table I using the corresponding weighted mean of the ANC value from Table II. The experimental data are taken from Ref. [23].

coupling modes by using the relation $C^2_{B;I} = [C_{B;j_B=3/2} + (-1)^I C_{B;j_B=1/2}]^2/2$ [14] and the averaged values of the $C^2_{B;j_B}$ derived in the present work. They are equal to $C^2_{B;I=1} = 0.104 \pm 0.010$ fm^{-1} and $C^2_{B;I=2} = 0.509 \pm 0.050$ fm^{-1}, which results in $S^{(I)}_{17}(0)/C^2_{B;I} = 3.685 \times 10^{-5}$ and 3.727×10^{-5} MeV b fm obtained from (8) for $I = 1$ and 2, respectively. From here and formulas (27) and (28) of Ref. [59], we obtain $a^{(I)}_0 \approx 23.2$ and 14.8 fm for the s-wave scattering length for $I = 1$ and 2, respectively, as well as the slope of $S_{17}(0)$ near $E = 0$ as $s^{(I)}_1 = S_{17}{}^{(I)\prime}(0)/S_{17}{}^{(I)}(0) \approx -2.2$ and -2.0 MeV^{-1} for $I = 1$ and 2, respectively. Using the values found for the scattering lengths at $I = 1$ and 2 in the formulas (29) and (30) of Ref. [59], we can obtain the values of the average scattering length $\bar{a}_o$ and then the value of the slope $s_1 = S'_{17}(0)/S_{17}(0)$. They are equal to be $\bar{a}_o \approx 16.2$ fm and $s_1 \approx -2.1$ MeV^{-1}. These results for $s^{(I)}_1$ and s_1 are close to those of $s^{(1)}_1 = -1.65$ MeV^{-1}, $s^{(1)}_1 = -1.77$ MeV^{-1}, and $s_1 = -1.74$ MeV^{-1}, which can be obtained from the above-mentioned polynomial approximation, as well as to those of $s_1 = -1.86$, -1.92, and -1.97 MeV^{-1} for the MN Volkov (V2) potentials [65], respectively. The slope of $S_{17}(0)$ near $E = 0$ determined in the present work becomes slightly steeper than that predicted in Refs. [59,65]. But, as is seen here, the s_1 values of Refs. [59,65] depend noticeably on the input potential. The values of $a^{(I)}_0$ ($I = 1$ and 2) and $\bar{a}_o$ obtained in the present work differ significantly from those derived in Refs. [20,59,66]. We note that the magnitudes of $a^{(I)}_0$ and $\bar{a}_o$ defined from the corresponding expressions of Ref. [59] are very sensitive to those of the ratios $S^{(I)}_{17}(0)/C^2_{B;I}$ and $S_{17}(0)/C^2_B$, where $S_{17}(0) = \sum_{I=1,2} S^{(I)}_{17}(0) = \sum_{j_B=1/2,3/2} S^{(j_B)}_{17}(0)$ and $C^2_B = \sum_{I=1,2} C^2_{B;I}$. The calculations showed that a small change of the ratios results in considerable change for $a^{(I)}_0$ and $\bar{a}_o$. For example, the values of $a^{(I)}_0 = 25$ and -8 fm at $I = 1$ and 2 as well as of $\bar{a}_o = -2.8$ fm obtained in Ref. [20] give the values of $S^{(I)}_{17}(0)/C^2_{B;I} = 3.677 \times 10^{-5}$ and 3.840×10^{-5} MeV b fm for $I = 1$ and 2, respectively, and $S_{17}(0)/C^2_B = 3.813 \times 10^{-5}$ MeV b fm. A similar situation occurs in the other above-mentioned works.

It follows that one of the main reasons of the observed discrepancy between the results of the present work and other works for the s-wave $p + {}^7$Be scattering lengths and the slope of $S_{17}(E)$ near $E = 0$ is the difference between the values of the ANCs and $S_{17}(0)$ derived by other authors and those obtained in the present work. From our point of view, our results for the s-wave $p + {}^7$Be scattering lengths and the slope of $S_{17}(E)$ near $E = 0$ are more reliable because they are derived with the minimum ambiguity connected with the ANC and $S_{17}(0)$ values.

IV. CONCLUSION

The scrupulous analysis of the ^{7}Be$(d,n)^8$B reaction data at $E_i = 4.5$ and 5.8 MeV is performed within the modified DWBA. It is demonstrated that the peripheral character of this reaction in the main peak region of the angular distributions occurs only for $E_i = 4.5$ MeV [23]. Therefore, the experimental differential cross sections of the reaction under consideration measured in Ref. [23] can be used as a source of determination of the squared ANC values C^2_B for $p + {}^7\text{Be} \to {}^8$B. A new value for the ANC was obtained, which is in agreement with that recommended in Refs. [10,54] and differs strongly from the value, which is deduced within the modified DWBA in Ref. [16] from the analysis of the other proton transfer reactions.

The value of the ANC from this work was used to estimate the astrophysical S factor at $E = 0$ and the value of $S_{17}(0)$ equal to 22.8 ± 2.2 eV b was obtained. Its averaged value is in excellent agreement with that recommended in Ref. [10], which nevertheless differs noticeably from that recommended in Refs. [8,16,21,23,51,52,55] and obtained by other authors from the data of the Coulomb breakup of ^{8}B into the proton and the ^{7}Be nucleus in the field of different multi-charged ions. Also, the new estimation is obtained for the s-wave scattering length for the $p + {}^7$Be scattering and the slope of $S_{17}(0)$ near $E = 0$.

ACKNOWLEDGMENTS

The authors are deeply grateful to L. D. Blokhintsev, V. S. Goldberg, A. M. Mukhamedzhanov, K. Ogata, and R. J. Peterson for discussions. The authors also appreciate the

anonymous referee's careful reading of the manuscript and constructive suggestions. The work was supported in part by the Academy of Sciences of the Republic of Uzbekistan (Grants No. F2-FA-F117 and No. F2-FA-F114).

[1] J. N. Bahcall, N. A. Bahcall, and R. K. Ulrich, Astrophys. J. **156**, 559 (1969).
[2] J. N. Bahcall, A. M. Serenelli, and S. Basu, Astrophys. J. **621**, L85 (2005).
[3] J. N. Bahcall, W. F. Huebner, S. H. Lubow, P. D. Parker, and R. K. Ulrich, Rev. Mod. Phys. **54**, 767 (1982).
[4] J. N. Bahcall and R. K. Ulrich, Rev. Mod. Phys. **60**, 297 (1988).
[5] J. N. Bahcall and M. H. Pinsonneault, Rev. Mod. Phys. **64**, 885 (1992).
[6] J. N. Bahcall, S. Basu, and M. H. Pinsonneault, Phys. Lett. B **433**, 1 (1998); Astrophys. J. **555**, 990 (2001).
[7] C. Rolfs and W. S. Rodney, *Cauldrons in the Cosmos* (University of Chicago Press, Chicago, 1988).
[8] E. G. Adelberger *et al.*, Rev. Mod. Phys. **83**, 195 (2011).
[9] R. Yarmukhamedov and Q. I. Tursunmahatov, *The Universe Evolution: Astrophysical and Nuclear Aspects* (Nova, New York, 2013), Chap. 6.
[10] S. B. Igamov and R. Yarmukhamedov, Phys. At. Nucl. **71**, 1740 (2008).
[11] N. K. Timofeyuk, D. Baye, and P. Descouvemont, Nucl. Phys. A **620**, 29 (1997).
[12] N. K. Timofeyuk, Nucl. Phys. A **632**, 19 (1998).
[13] P. Descouvemont, Phys. Rev. C **70**, 065802 (2004).
[14] L. D. Blokhintsev, I. Borbely, and E. I. Dolinskii, Fiz. Elem. Chastits At. Yadra **8**, 1189 (1977) [Sov. J. Part. Nucl. **8**, 485 (1977)].
[15] S. B. Igamov and R. Yarmukhamedov, Nucl. Phys. A **781**, 247 (2007); **832**, 346 (2010).
[16] G. Tabacaru, A. Azhari, J. Brinkley *et al.*, Phys. Rev. C **73**, 025808 (2006).
[17] A. Azhari, V. Burjan, F. Carstoiu *et al.*, Phys. Rev. Lett. **82**, 3960 (1999).
[18] A. Azhari, V. Burjan, F. Carstoiu *et al.*, Phys. Rev. C **60**, 055803 (1999).
[19] S. B. Igamov, M. C. Nadyrbekov, and R. Yarmukhamedov, Phys. At. Nucl. **70**, 1694 (2007).
[20] K. Ogata, S. Hashimoto, Y. Iseri, M. Kamimura, and M. Yahiro, Phys. Rev. C **73**, 024605 (2006).
[21] A. R. Junghans, M. C. Mohrmann, K. A. Snover *et al.*, Phys. Rev. C **68**, 065803 (2003).
[22] Weiping Liu *et al.*, Phys. Rev. Lett. **77**, 611 (1996).
[23] J. J. Das *et al.*, Phys. Rev. C **73**, 015808 (2006).
[24] K. Ogata, M. Yahiro, Y. Iseri, and M. Kamimura, Phys. Rev. C **67**, 011602(R) (2003).
[25] S. A. Goncharov, J. Dobesh, E. I. Dolinskii, A. M. Mukhamedzhanov, and J. Cejpek, Yad. Fiz. **35**, 662 (1982) [Sov. J. Nucl. Phys. **35**, 383 (1982)].
[26] A. Deltuva, Phys. Rev. C **92**, 064613 (2015).
[27] O. R. Tojiboev, R. Yarmukhamedov, S. V. Artemov, and M. Kayumov, Uzb. J. Phys. **16**, 247 (2014).
[28] I. R. Gulamov, A. M. Mukhamedzhanov, and G. K. Nie, Yad. Fiz. **58**, 1789 (1995).
[29] S. V. Artemov, I. R. Gulamov, E. A. Zaparov *et al.*, Yad. Fiz. **59**, 454 (1996) [Phys. Atom. Nucl. **59**, 428 (1996)].
[30] A. M. Mukhamedzhanov, H. L. Clark, C. A. Gagliardi *et al.*, Phys. Rev. C **56**, 1302 (1997).
[31] K. R. Greider and L. R. Dodd, Phys. Rev. **146**, 671 (1966).
[32] N. Austern, R. M. Drisko, E. C. Halbert, and G. R. Satchler, Phys. Rev. **133**, B3 (1966).
[33] Sh. S. Kajumov, A. M. Mukhamedzhanov, and R. Yarmukhamedov, Z. Phys. A **331**, 335 (1988).
[34] A. M. Mukhamedzhanov, I. Borbely *et al.*, Izv. AN SSSR, Ser. Fiz. **48**, 350 (1984).
[35] R. M. DeVries, Ph.D. thesis, Ubiversity of California, 1971; J. Perrenoud and R. M. DeVries, Phys. Lett. B **36**, 18 (1971).
[36] L. Trache, A. Azhari, F. Carstoiu *et al.*, Phys. Rev. C **67**, 062801(R) (2003).
[37] X. D. Liu, M. A. Famiano, W. G. Lynch, M. B. Tsang, and J. A. Tostevin, Phys. Rev. C **69**, 064313 (2004).
[38] H. Lüdecke, Tan Wan-Tjin *et al.*, Nucl. Phys. A **109**, 676 (1968).
[39] M. Avrigeanu, W. von Oertson, U. Fischer, and V. Avrigeanu, Nucl. Phys. A **759**, 327 (2005).
[40] C. M. Perey and F. G. Perey, At. Data Nucl. Data Tables **17**, 1 (1976).
[41] P. Pereslavtsev, U. U. Fischer, S. Simakov, and M. Avrigeanu, Nucl. Instrum. Methods B **266**, 3501 (2008).
[42] W. Fitz, R. Jahr, and R. Santo, Nucl. Phys. A **101**, 449 (1967).
[43] J. P. Schiffer, G. C. Morrison, R. N. Siemsson, and B. Zeidman, Phys. Rev. **164**, 1274 (1967).
[44] F. M. Nunes and A. M. Mukhamedzhanov, Phys. Rev. C **64**, 062801(R) (2001).
[45] N. Burtebaev, J. T. Burtebaeva, N. V. Glushchenko, Zh. K. Kerimkulov, A. Amar, M. Nassurulla, S. B. Sakuta, S. V. Artemov, S. B. Igamov, A. A. Karakhodzhaev, K. Rusek, and S. Kliczewski, Nucl. Phys. A **909**, 20 (2013).
[46] I. J. Thompson, FRESCO, Department of Physics, University of Surrey, July 2006, Guildford GU2 7XH, England, version FRESCO 2.0 [http://www.fresco.org.uk/].
[47] E. I. Dolinsky, P. G. Dzhamalov, and F. V. Mukhmedzhanov, Nucl. Phys. **202**, 97 (1973).
[48] L. D. Blokhintsev, E. I. Dolinsky, and V. S. Popov, Nucl. Phys. **40**, 117 (1963).
[49] N. Burtebaev, A. Duisebaev, B. A. Duisebaev, G. I. Ivanov, and S. B. Sakuta, Yad. Fiz. **59**, 33 (1996) [Phys. Atom. Nucl. **59**, 29 (1996)].
[50] C. Angulo, M. Arnould, M. Rayet *et al.*, Nucl. Phys. A **656**, 3 (1999).
[51] J. T. Huang, C. A. Bertulani, and V. Guimarães, At. Data Nucl. Data Tables **96**, 824 (2010).
[52] F. C. Barker, Nucl. Phys. A **588**, 693 (1995).
[53] L. Trache, F. Carstoiu, C. A. Gagliardi, and R. E. Tribble, Phys. Rev. Lett. **87**, 271102 (2001).
[54] T. L. Belyaeva, E. F. Aguilera, E. Martinez-Quiroz, A. M. Moro, and J. J. Kolata, Phys. Rev. C **80**, 064617 (2009).
[55] L. T. Baby, C. Bordeanu, G. Goldring *et al.*, Phys. Rev. Lett. **90**, 022501 (2003); Phys. Rev. C **67**, 065805 (2003).
[56] F. C. Barker, Aust. J. Phys. **33**, 177 (1980); Phys. Rev. C **28**, 1407 (1983).
[57] E. O. Alt, B. F. Irgaziev, and A. M. Mukhamedzhanov, Phys. Rev. Lett. **90**, 122701 (2003).
[58] D. Baye and E. Brainis, Phys. Rev. C **61**, 025801 (2000).
[59] D. Baye, Phys. Rev. C **62**, 065803 (2000).
[60] N. Iwasa, F. Boué, G. Surówka *et al.*, Phys. Rev. Lett. **83**, 2910 (1999).

[61] F. Schümann, F. Hammache, S. Typel *et al.*, Phys. Rev. Lett. **90**, 232501 (2003).
[62] B. Davids and S. Typel, Phys. Rev. C **68**, 045802 (2003).
[63] F. Schümann, S. Typel, F. Hammache *et al.*, Phys. Rev. C **73**, 015806 (2006).
[64] B. K. Jennings, S. Karataglidis, and T. D. Shoppa, Phys. Rev. C **58**, 3711 (1998).
[65] F. C. Barker, Nucl. Phys. A **768**, 241 (2006).
[66] C. Angulo, M. Azzouz, P. Descouvemont *et al.*, Nucl. Phys. A **716**, 211 (2003).